

# A Goniophotometric System for Measuring Object Surface Reflection Using Robot Arms

Akira Kimachi

Osaka Electro-Communication University  
18-8 Hatsu-cho, Neyagawa, Osaka 572-8530, Japan  
kima@isc.osakac.ac.jp

Norihiro Tanaka

Nagano University  
658-1 Shimonogo, Ueda, Nagano 386-1298, Japan  
n-tanaka@nagano.ac.jp

Masataka Tatsumi

Osaka Electro-Communication University  
18-8 Hatsu-cho, Neyagawa, Osaka 572-8530, Japan  
tatsumi@tmlab.osakac.ac.jp

Shoji Tominaga

Osaka Electro-Communication University  
18-8 Hatsu-cho, Neyagawa, Osaka 572-8530, Japan  
shoji@tmlab.osakac.ac.jp

## Abstract

*This paper proposes a goniophotometric system for measuring light reflection on an object surface using two commercial robot arms and a digital camera. It allows four degrees of freedom in incident and viewing angles necessary for full parametrization of a reflection model. Collected images are transformed as if they were all captured from the same viewing direction. A database of measured surface reflection is then constructed directly from the pixel values of the transformed images at each individual point on the object surface for a whole set of incident and viewing angles. From the collected image database, the parameters for the Torrance-Sparrow surface reflection model, such as diffuse reflectance, specular reflectance and surface roughness, are estimated. The proposed system enables two-dimensional pixel-wise measurement and modeling of surface reflectance, and thus, can deal with objects with spatially nonuniform surface reflectance. Experiments were performed on colored polyvinyl chloride sheets. The estimated Torrance-sparrow reflection models showed good agreement with the measurement data obtained by the proposed system.*

## 1 INTRODUCTION

Modeling light reflection on an object surface provides useful information both in computer vision and in computer graphics. For example, light reflected from an object surface includes a lot of information on the surface properties such as surface reflectance and surface roughness. Accurate modeling of light reflection allows us rendering realistic images of an object under any illumination and observation conditions. It is therefore an important task to determine a 3D reflection model based on measurement that represents the actual reflection behavior of an object.

Toward this problem, we first proposed an algorithm for estimating various reflectance parameters of the Phong reflection model from a single RGB image [1]. We then devised a measurement apparatus consisting of a collimated white light source, a turntable to place the object on, and a six-channel spectral camera on a rotating arm [2]. From the obtained multi-band images we estimated the parameters of the Torrance-Sparrow reflection model, which is considered more realistic than the Phong model. We extended this method to estimate the refractive index of an inhomogeneous dielectric object and successfully

rendered realistic images using estimated parameters [3]. One problem with the proposed measurement apparatus is that it had only two degrees of freedom in incident and viewing directions with a limited working range of the camera arm.

To solve this problem, we propose a goniophotometric system for measuring light reflection on an object surface using two commercial robot arms and a digital camera. It allows four degrees of freedom in incident and viewing angles necessary for full parametrization of a reflection model. Collected images are transformed as if they were all captured from the same viewing direction. A database of measured surface reflection is then constructed directly from the pixel values of the transformed images at each individual point on the object surface for a whole set of incident and viewing angles. Once the database is available, we can estimate the parameters for the Torrance-Sparrow surface reflection model such as diffuse reflectance, specular reflectance and surface roughness.

In comparison to other methods for measuring surface reflection, our system takes the approach of multi-point measurement as employed by Sato *et al.*[4] and Dana *et al.*[5] in that it uses image pixels to sample points on the surface of the object, not to sample viewing angles as employed by Matusik *et al.*[6] and Marschner *et al.*[7]. This approach enables our system to deal with objects of spatially nonuniform reflectance.

## 2 GONIOPHOTOMETRIC SYSTEM FOR REFLECTION MEASUREMENT

### 2.1 System Overview

Figure 1 shows a photograph of the proposed goniophotometric measurement system consisting of two robot arms with six joints, a fixed light source illuminating from a horizontal direction, and a digital camera. One of the robot arm (Mitsubishi Electric RV-4A) holds an object on its end and rotates it around a point on the surface of the object to change its pose with three degrees of freedom (3DOF). This movement is difficult to realize without this kind of multi-joint robot arm. The other robot arm (Mitsubishi Electric RV-2A) hangs down a 10-bit monochrome digital CCD camera (Tokyo Electronic Industry CS3920) from its end and rotates it in a horizontal direction to give 1DOF.

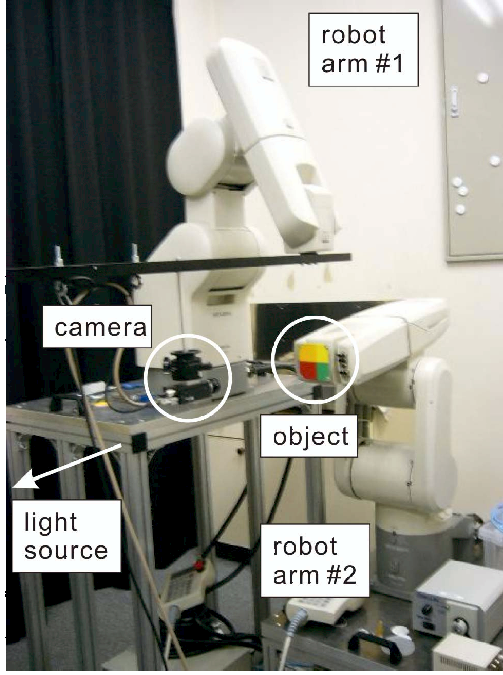


Figure 1. Photograph of the goniophotometric system for measuring light reflection on an object surface using two robot arms, a digital camera, and a light source.

The pose and position of the robot arms are related to the incident polar and azimuth angles  $(\theta_i, \phi_i)$  of the light and the viewing polar and azimuth angles  $(\theta_e, \phi_e)$  of the camera as follows. Figure 2 illustrates the geometry for goniophotometric measurement. Denoting the pose of the object by Euler angles  $(\phi_1, \theta_1, \psi_1)$  and the pose and position of the camera center by a horizontal rotation angle  $\theta_2$  and a translation vector  $\mathbf{T}_2$ , respectively, all defined in the  $XYZ$  world coordinate system, the relative position and pose of the camera center with respect to the object surface is given by a matrix in a homogeneous representation (1)

$$\mathbf{M} = \mathbf{M}_1^{-1} \mathbf{M}_2 = \begin{bmatrix} \mathbf{R}_1^{-1}(\phi_1, \theta_1, \psi_1) \mathbf{R}_2(\theta_2) & \mathbf{R}_1^{-1}(\phi_1, \theta_1, \psi_1) \mathbf{T}_2 \\ \mathbf{0}^T & 1 \end{bmatrix} \quad (1)$$

where

$$\mathbf{M}_1 = \begin{bmatrix} \mathbf{R}_1(\phi_1, \theta_1, \psi_1) & \mathbf{0} \\ \mathbf{0}^T & 1 \end{bmatrix}, \mathbf{M}_2 = \begin{bmatrix} \mathbf{R}_2(\theta_2) & \mathbf{T}_2 \\ \mathbf{0}^T & 1 \end{bmatrix} \quad (2)$$

and  $\mathbf{R}_1(\phi_1, \theta_1, \psi_1)$  and  $\mathbf{R}_2(\theta_2)$  denote rotation matrices defined by the Euler angles  $(\phi_1, \theta_1, \psi_1)$  and the horizontal rotation angle  $\theta_2$ , respectively. The incident angles  $(\theta_i, \phi_i)$  of the light are then computed from the rotation part of  $\mathbf{M}_1^{-1}$ , which transforms a world coordinate representation of position and pose to an object-centered representation, and from the unit vector pointing to the incident direction  $\mathbf{n}_i = [1, 0, 0]^T$ . Similarly, the viewing angles  $(\theta_e, \phi_e)$  of the camera are obtained from  $\mathbf{M}^{-1}$ , which transforms a camera-centered representation to an object-centered one, and from the unit vector pointing to the viewing direction  $\mathbf{n}_e = [\cos \theta_e, \sin \theta_e, 0]^T$ .

Images of an object surface are captured by independently combining the incident and viewing directions. To

record specularly reflected light without saturation while keeping diffusely reflected light well above the noise level, we extend the effective dynamic range of the camera from 10 to 12 bits by capturing three consecutive images of the same scene with the shutter speed doubled after every acquisition and by combining them into a single 12-bit image.

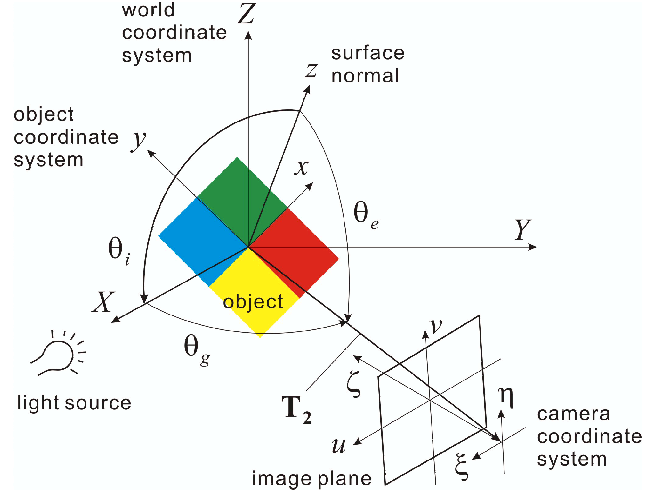


Figure 2. Geometry of a target object, light source and camera in the goniophotometric measuring system.

## 2.2 Image Registration for Pixelwise Reflection Modeling

The reflection model is estimated at each pixel point on the object surface from the database of images collected by the goniophotometric system. It is therefore necessary to assign a reflectance value to each point on the object surface for any incident and viewing directions. This can be done by registering the images as if they were all taken from the same viewing direction with respect to the object. For this purpose, we transform the images so that the coordinate axes of the image plane go parallel to the  $x$  and  $y$  axes of the object coordinate system.

Figure 3 illustrates the geometry of this transformation. Assuming that the  $\xi\eta$ -plane of the camera-centered coordinate system after transformation, being also parallel to the image plane, is separated by a distance  $z_0$  from the  $xy$ -plane, we find that a pixel  $(u, v)$  of the image after transformation corresponds to a point  $(\xi, \eta, z_0)$  on the object in the camera-centered coordinate system, which also corresponds to a point  $(-x, y, 0)$  in the object coordinate system, as

$$\begin{bmatrix} \xi \\ \eta \\ z_0 \end{bmatrix} = \begin{bmatrix} -x \\ y \\ z_0 \end{bmatrix} = z_0 \mathbf{A}^{-1} \begin{bmatrix} u \\ v \\ 1 \end{bmatrix}, \quad (3)$$

where  $(\xi, \eta) = (-x, y)$  by assumption and  $\mathbf{A}$  denotes a  $3 \times 3$  matrix for perspective projection [8].

Furthermore, the point  $(x, y)$  on the  $xy$ -plane of the object coordinate system is observed at a pixel  $(u', v')$  of the original image before transformation as

$$\begin{bmatrix} su' \\ sv' \\ s \end{bmatrix} = \mathbf{A} \mathbf{R}_2^{-1}(\theta_2) \left\{ \mathbf{R}_1(\phi_1, \theta_1, \psi_1) \begin{bmatrix} x \\ y \\ 0 \end{bmatrix} - \mathbf{T}_2 \right\}. \quad (4)$$

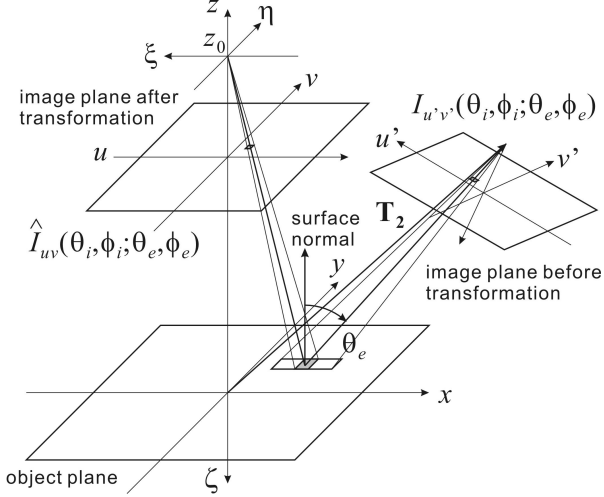


Figure 3. Geometry of the image planes with respect to the object during the image transformation.

Substituting  $(x, y)$  in Eq. (3) into Eq. (4) then yields the pixel position  $(u', v')$  of the original image that is mapped to a pixel  $(u, v)$  of the new image after transformation. Thus, the pixel value of the transformed image  $\hat{I}_{uv}(\theta_i, \phi_i; \theta_e, \phi_e)$  is related to that of the original one  $I_{u',v'}(\theta_i, \phi_i; \theta_e, \phi_e)$  as

$$\hat{I}_{uv}(\theta_i, \phi_i; \theta_e, \phi_e) = I_{u',v'}(\theta_i, \phi_i; \theta_e, \phi_e). \quad (5)$$

Note that the viewing angles  $(\theta_e, \phi_e)$ , which may be different from those of the optical axis of the camera due to perspective projection and also to alignment error of the two robot arms and the camera, should be computed from the actual viewing angle of the pixel  $(u', v')$ . Since  $(u', v')$  usually does not coincide with an image grid point, bilinear interpolation is employed to compute  $\hat{I}_{uv}(\theta_i, \phi_i; \theta_e, \phi_e)$  in this study.

### 2.3 Camera Calibration

To compute  $(u', v')$  by Eqs. (3) and (4), we have to know the matrix  $\mathbf{A}$ , which consists of intrinsic camera parameters such as pixel spacing and focal length. We obtain  $\mathbf{A}$  with a camera calibration method proposed by Zhang [8], which also yields the matrix  $\mathbf{M}$  in Eq. (1) representing the camera position and pose relative to the object, referred to as extrinsic camera parameters, for each image.

One problem with this measurement system is that, since the two robot arms and the light source are separate apparatuses, it is difficult to make the optical axis of the camera and the rotation centers of the two robot arms coincide. This implies that at every point on the surface of the object observed by a pixel of the camera, the actual incident direction  $(\theta_i, \phi_i)$  of the light source and viewing direction  $(\theta_e, \phi_e)$  of the pixel relative to the object can have errors with respect to the nominal geometry setting predetermined by the pose of the robot arms.

Assuming no errors on the incident direction of the illumination, we only consider estimating the actual viewing direction of the camera. We obtained a look-up table (LUT) of the actual camera positions and poses for a wide range of angles  $\theta_g$  from the extrinsic parameter matrices  $\mathbf{M}$ , again using the Zhang's calibration method [8].

## 3 ESTIMATION OF REFLECTION MODEL PARAMETERS

As in the previous work [2][3], we are particularly interested in the Torrance-Sparrow reflection model in terms of balance between complexity and accuracy. From the registered images  $\hat{I}_{uv}(\theta_i, \phi_i; \theta_e, \phi_e)$ , we estimate the parameters of the Torrance-Sparrow model at each point of the object surface. Assuming that the incident irradiance is spatially uniform as given by  $E_{uv}(\theta_i, \phi_i) = E_0 \cos \theta_i$ , we formulate the reflection model at a point on the object surface observed by a pixel  $(u, v)$  in the transformed image, in terms of image irradiance normalized by  $E_0$ , as

$$Y_{uv}(\theta_i, \phi_i; \theta_e, \phi_e) = \alpha_{uv} S_{uv} \cos \theta_i + \beta_{uv} \frac{F(\theta_i; n_{uv}, \kappa_{uv}) D(\phi_g, \gamma_{uv})}{\cos \theta_e}, \quad (6)$$

where

$S_{uv}$ : diffuse reflectance;

$F(\theta_i; n_{uv}, \kappa_{uv})$ : Fresnel coefficient dependent on the complex refractive index  $n_{uv} + j\kappa_{uv}$ ;

$D(\phi_g, \gamma_{uv}) = \exp(-\ln 2 \cdot \phi_g^2 / \gamma_{uv}^2)$ : gloss factor

$\phi_g$ : angle between the surface normal and the bisector of the incident and viewing direction vectors; and

$\alpha_{uv}, \beta_{uv}$ : coefficients denoting the fraction of incident energy.

We estimate the parameters  $\alpha_{uv}, \beta_{uv}, \gamma_{uv}, n_{uv}$  either at each single pixel or in regions covering multiple pixels within the domain of the registered images  $\hat{I}_{uv}(\theta_i, \phi_i; \theta_e, \phi_e)$  by minimizing the error functional

$$J = \sum_{u,v} [Y_{uv}(\theta_i, \phi_i; \theta_e, \phi_e) - \hat{I}_{uv}(\theta_i, \phi_i; \theta_e, \phi_e)]^2. \quad (7)$$

To minimize Eq. (7), we employ a nonlinear estimation algorithm such as the Levenberg-Marquardt algorithm, or perform exhaustive search over a number of combinations of the parameters.

## 4 ESTIMATION RESULTS OF SURFACE REFLECTION

We measured surface reflection on a flat object consisting of four patches of colored polyvinyl chloride (PVC) sheets, as shown in the top-left photograph in Fig. 4. The results are also shown by the curves in Fig. 4, which plots average pixel values of the camera output images over 20x20 pixels within each patch of the object. During the measurement, the incident angle  $\theta_i$  of the light source was varied from 30° to 65° in 5° steps. For each  $\theta_i$ , the viewing angle  $\theta_e$  of the camera was changed from 0° to 80° in 5° steps except in the vicinity of the specular reflection angle  $\theta_e = \theta_i$ , where the scanning step was set to 0.5° over  $\pm 15^\circ$  on both sides. As mentioned in Sec. 2.3,  $\theta_e$  was corrected to the actual viewing angle for each 20x20-pixel region with the LUT obtained by calibration.

From the measurement results in Fig. 4, we estimated the parameters  $n_{uv}, \alpha_{uv}, \beta_{uv}$  and  $\gamma_{uv}$  of the Torrance-Sparrow model by minimizing  $J$  in Eq. (9) by an exhaustive search method. Table 1 shows the estimated parameters for all color patches of the object. While the diffuse and specular coefficients  $\alpha_{uv}, \beta_{uv}$  have different

values, the refractive index  $n_{mv}$  and the gloss parameter  $\gamma_{mv}$  each have similar values for all patches, which agrees with the fact that the patches are all made of PVC.

In Fig. 5 we separately depicted the estimation results for patch C by plotting Torrance-Sparrow curves for the estimated parameters along with the measurement results. The curves are in good agreement especially for small incident angles  $\theta_i$ . The slightly different amount of shift along the abscissa are considered to have resulted from the difference in actual incident angle at the 20x20-pixel target regions on the object due to insufficient collimation of the light source.

## 5 SUMMARY

We have developed a goniophotometric system for measuring surface reflection on an object using two commercial robot arms and a digital camera. Using this system we measured the light reflection on an object surface consisting of colored PVC patches and estimated the parameters of the Torrance-Sparrow model at several locations on the object surface. The experimental results of reflection measurement and model estimation have confirmed the feasibility of the proposed measurement system and modeling algorithm.

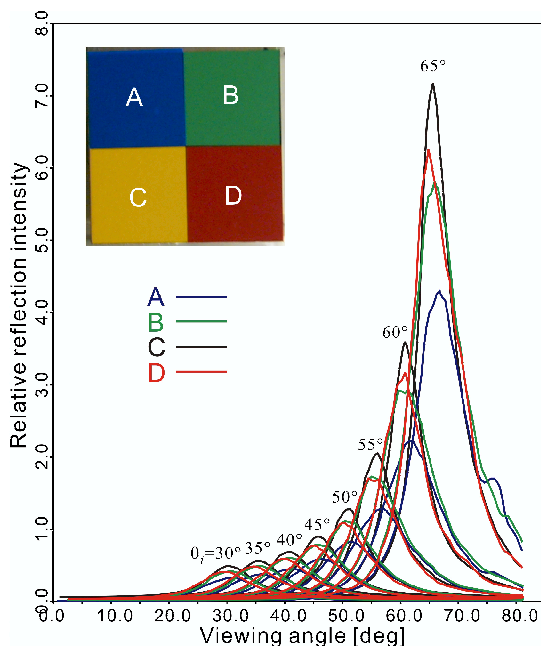


Figure 4. Results of surface reflection measurement by the proposed system for an object consisting of four colored PVC patches (top-left photograph).

## References

- [1] S. Tominaga and N. Tanaka, "Estimating reflection model parameters from a single color image," *IEEE Comput. Graph. Appl.*, **20**(15), pp. 58-66 (2000).
- [2] N. Tanaka and S. Tominaga, "Measurement of surface reflection properties," in *IS&T/SID 9<sup>th</sup> Color Imaging*

*Conference*, pp. 52-55 (2001).

- [3] S. Tominaga and N. Tanaka, "Refractive index estimation and color image rendering," *Pattern Recognition Letters*, **24**, pp.1703-1713 (2003).
- [4] Y. Sato *et al.*, "Object shape and reflectance modeling from observation," *ACM SIGGRAPH '97, Comput. Graphics*, **31**, pp. 379-387 (1997).
- [5] K. J. Dana *et al.*, "Reflectance and texture of real-world surfaces," *ACM Trans. Graphics*, **18**(1), pp. 1-34 (1999).
- [6] W. Matusik *et al.*, "A data-driven reflectance model," *ACM SIGGRAPH '03, ACM Trans. Graphics*, **22**(3), pp. 759-769 (2003).
- [7] S. R. Marschner *et al.*, "Image-based bidirectional reflectance distribution function measurement," *Appl. Opt.*, **39**(16), pp. 2592-2600 (1999).
- [8] Z. Zhang, "Flexible camera calibration by viewing a plane from unknown orientations," in *Proc. of ICCV '99*, pp. 666-673 (1999).

Table 1. Parameters of the Torrance-Sparrow model estimated from the measurement results in Fig. 4.

Patch	$n_{mv}$	$\alpha_{mv}$	$\beta_{mv}$	$\gamma_{mv}$
A	1.49	2.3	$1.4 \times 10^3$	$5.8 \times 10^{-2}$
B	1.44	3.7	$1.7 \times 10^3$	$5.2 \times 10^{-2}$
C	1.43	17	$2.8 \times 10^3$	$3.8 \times 10^{-2}$
D	1.38	8.5	$2.5 \times 10^3$	$4.7 \times 10^{-2}$

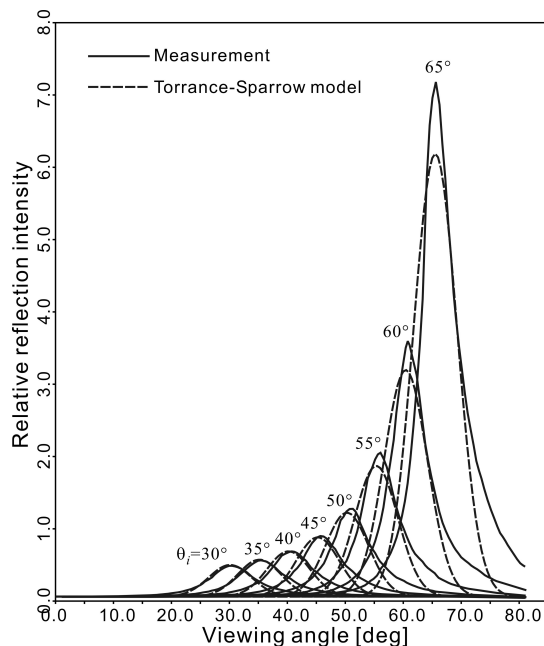


Figure 5. Torrance-Sparrow curves (dashed lines) for patch C of the PVC object, estimated from the results of surface reflection measurement (solid lines) in Fig. 4.